Chapter

Catalytic Behavior of Metal Active Sites From Modified Mesoporous Silicas in Oxidation of Organic Compounds

Viorica Parvulescu

Abstract

The ordered mesoporous silicas containing transition metals are versatile catalytic materials for oxidation of a wide range of organic compounds. In order to obtain active catalysts, different active redox metal sites have been introduced into specific locations (mesoporous channels and framework) of ordered mesoporous silicas (OMSs). All the reported results evidenced that localization of metal ions, their interaction with another metal (bimetallic catalysts) and the support, with typical properties of the ordered mesoporous silica, influenced the oxidation state, respectively their redox properties. To support this, the results regarding the specific properties of transitional metals in the ordered structure of silica, obtained using various characterization methods, were presented. The activity of metal sites in the oxidation reactions was evidenced in various applications carried out in the liquid or gaseous phase. The oxidation of various organic compounds in liquid phase with H_2O_2 (especially aromatic compounds and of alcohols) and in gas phase with oxygen from air was presented for a variety of metal-modified OMSs. The active sites and possible reaction mechanisms were presented for some catalytic systems. The immobilization of multiple metal active species on new ordered porous frameworks and their synergistic interactions remain topics of interest in the future.

Keywords: redox metal sites, transition metals, mesoporous silicas, oxidation reactions

1. Introduction

The ordered mesoporous silicas (OMSs) containing transition metals are versatile catalytic materials for oxidation of a wide range of organic compounds [1–3]. Mesoporous materials with various structures such as MCM-41 (2d hexagonal p6mm) [4–6], MCM-48 (3d cubic Ia3d) [7, 8], SBA-15 (large-pore 2d hexagonal p6mm) [2, 9–12], SBA-16 (large-pore 3d cubic Im3m) [13], KIT-5 (well-ordered cage-type mesoporous with cubic Fm3m) [2], and KIT-6 (large-pore cubic with interpenetrated cylindrical mesopores Ia3d) [2, 14–18] have been used as supports for transition metals. These supports with controlled morphology and accessible metallic center for the reactant molecules also offered the opportunity to

immobilize the transition metal complexes and their heterogenization [19, 20]. These catalysts have attracted much interest due to the desirable characteristics of the silica supports such as narrow pore size, high surface area and large pore volume, tunable mesoporous channels with well-defined pore-size distribution, controllable wall composition, and modifiable surface properties. Pore diameter of mesoporous silicas (2–50 nm) and porous structure are usually tailored by the choice of the template surfactant or the incorporation of swelling agents to expand the surfactant micelles during synthesis [21, 22]. In condition of typical synthesis environment of the mesoporous molecular supports, the incorporation of metal methods varies with properties of their precursors.

In order to obtain active catalysts, different active redox metal sites have been introduced into specific locations (mesoporous channels and framework) of the OMSs supports by direct synthesis methods (framework substitution) or post-synthetic methods. In any case, Me^{n+} can be simultaneously present in different coordination geometries and positions (surface, lattice) [16, 23]. In a direct-synthesis preparation, the condensations of silicon and metal species around the organic micelles occur simultaneously, and it is likely that some of the metal species are trapped in the silica walls during the formation of OMSs supports. This may influence the unit cell parameters, the wall thickness, and the long-range ordering of the material. By contrast, metal species introduced by a postsynthesis treatment (template ion exchange, impregnation, grafting, chemical vapor deposition methods) are mostly located at the surface of the mesopores and do not modify the internal composition of the silica walls, mainly when the samples are prepared in alcohol. The synthesis method offers the advantage that the dispersion and location of metal species are easily controlled. This may be a great advantage with respect to conventional synthesis methods to prepare materials with specific applications in catalysis. The activity of the obtained materials was demonstrated in various reactions, mostly oxidation reactions of the organic compounds in the liquid or gaseous phase. All the reported results show that the localization of the metal ion, morphology, particle and pore channel sizes and their interaction with the support, and other metal (bimetallic catalysts) influence the oxidation state of the catalytic sites, respectively their redox properties. Therefore, the redox properties of these materials are the result of the support and metal cation synergistic effect.

2. Location, chemical state, and environment of the incorporated metals

Catalytic properties of the incorporated transition metals in OMSs supports were mainly attributed to their location, chemical state, and environment. The location of metals in mesoporous silica network is the result of the synthesis method, the intrinsic properties of the incorporated metal, and silica support. The location, the loading, and the properties of the incorporated metals can also influence the support mesoporous structure. Thus, the variation of (100) peak in X-ray diffractograms obtained at a lower angle has been detected in many Me-MCM-41 patterns, indicating the effect of metal species on the ordered mesoporous structure of the support [3, 24, 25]. The higher concentrations of metal species (Me[(OH)n(H_2O)m]) at the interface affect the electrostatic interaction between surfactant and silica precursor and the polymerization processes of the silica system in alkaline media (pH 11) during synthesis. In such conditions, the free energy of the mesostructure formation decreases and a mixture of nonstructurated oxides (SiO_2–Co_3O_4) was exhibited [25]. Changing the Si-O-Si bond angle due to incorporation of metal in the mesoporous silica support increases the number of local defects within the mesoporous structure. IR spectroscopy is one of the first techniques that has been used for

the characterization of materials with metal incorporated in mesoporous silica to obtain information on changes of the Si-OH from surface or regarding appearance of the new vibrations as (Si-O-Me). The change in the Si-O-Si bond angle due to incorporation of Me increases the number of local defects within the mesoporous structure. A much disputed is the change in intensity of the band at 960 cm^{-1} indicating the structural changes in the Si-OH surface due to the presence of metal oxide or to the evolution of new vibrations (Si-O-Me) that appear in the same region [26].

For TiMCM-41 synthesized by surfactant-assisted direct hydrothermal (DHT) method [7, 16, 21], the absence of the characteristic bands for crystalline TiO_2 phase in the wide angle XRD patterns reveal that the metal ions were either atomically dispersed in MCM-41 framework or may exist in an amorphous dispersed form on the outside surface of mesoporous support. Diffuse reflectance UV–Vis spectra also revealed distorted tetrahedral environments for titanium inside the MCM-41 matrix or octahedrally coordinated titanium sites, due to the possible hydration effects. The presence of titanium in various mesoporous silica supports in +4 oxidation state was confirmed by ESR and XPS analysis [7, 9, 23]. XPS analysis was used as an additional tool of UV–VIS data since the dispersion of Ti species depends strongly on the synthesis method, properties of the support, and other metals [7, 9, 16]. XRD and spectroscopic results reveal that the titanium was dispersed as titanium ions on SBA-15 silica wall surfaces at low titanium loading, whereas a titanium dioxide anatase film was formed at high titanium loading [16, 23]. Thus, the nature of Ti species on TiMCM-41 s surface, prepared by three different methods, i.e., isomorphous substitution, wet impregnation, and mechanical mixing, was analyzed by means of Raman spectra [27]. The obtained results indicated the presence of anatase for TiO_2MCM-41 sample obtained by mechanical mixing. In contrast, no Raman-active bands were observed on TiMCM-41, obtained by direct synthesis, indicating the absence of surface anatase phase. For TiMCM-41, obtained by impregnation method, no surface anatase phase was detected at a low Ti/Si ratio of 0.3, while surface anatase was detected at high Ti/Si ratios such as 0.6 and 0.9. UV–Vis spectra showed for TiMCM-41 a strong absorbance band at 210 nm and a shoulder band at 260 nm. The first was attributed to isolated Ti atoms in tetrahedral coordination, while the band at 260 nm was attributed to isolated Ti atoms in pentahedral or octahedral coordination. Therefore, it is believed most Ti atoms should substitute Si in the framework or surface in TiMCM-41 with the formation of Ti-O-Si-O-Ti bands. For TiO_2MCM-41, adsorption bands at 220, 260, and 320 nm were clearly observed in the UV–vis spectra. The band at 320 nm was typical for bulk titania, indicating the existence of bulk TiO_2. The band at 220 was attributed to isolated Ti atoms with distorted tetrahedral environment. These Ti species, dispersed on OMSs support, were supported along with other cations (Ce, V, Nb) or was used as support for another active metal as Ce, Pt, Fe [7, 9, 16, 21, 28]. The second or third [16] metal was evidenced by SEM backscattering and TEM microscopy, as extra framework nanoparticles (**Figure 1**). A good correlation between TEM results (**Figure 1C**) and H_2 chemisorption on Pt nanoparticles' diameter was observed.

XPS spectroscopy sustained the interaction of the second metal with titanium [29] and together on the third metal [16]. The presence of Pt^0 on surface and the effects of titanium loading and of cerium on its percent were explained by metal-support interaction considering TiKIT-6 and CeTiKIT-6 samples as supports for Pt (**Figure 2**). Due to Ti and Ce redox properties and strong interaction with noble metals, these metal oxides influence Pt/PtO molar ratio on the catalyst surface. The extended X-ray absorption fine structure measurements evidenced for Pt immobilized on SBA-15, in absence of Ti and Ce species, the presence of Pt–oxygen chemical bonds at the surface. The concentration of these Pt species increased for Pt-amino-SBA-15 sample [11].

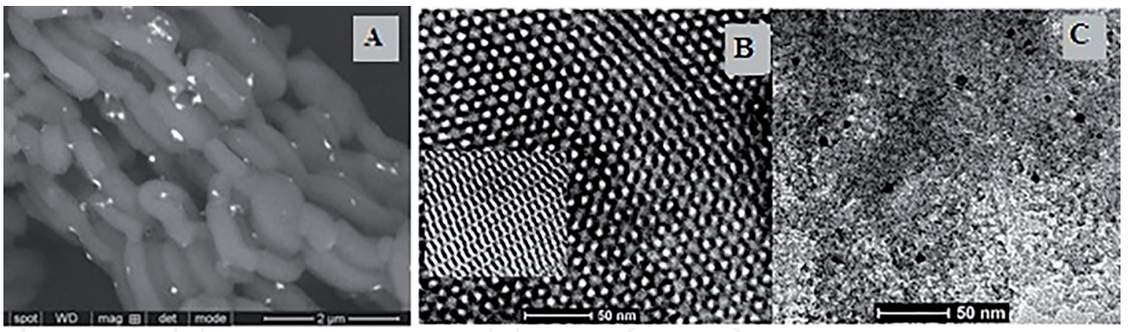

Figure 1.
SEM backscattering (A) of PtTi-SBA-15 (unpublished) and TEM images of TiKIT-6 (B) and PtTiKIT-6 (C) samples (with permission from Ref. [16]).

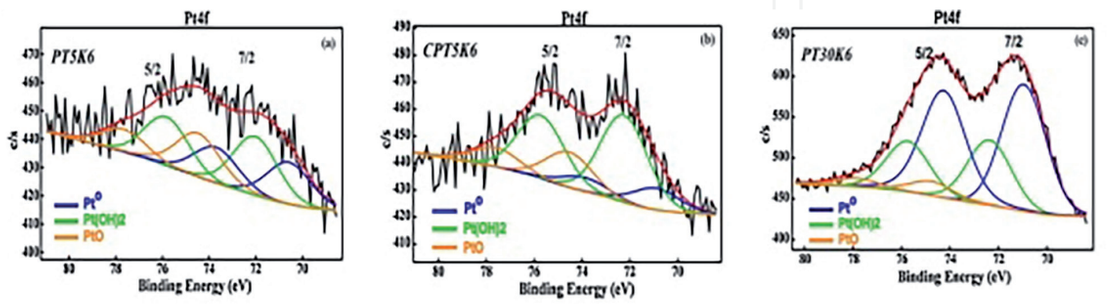

Figure 2.
XPS spectra Pt-modified KIT-6 mesoporous silica and Pt species atomic percent (with permission from Ref. [16]).

Another transition metal that is present as active component in OMSs supports was vanadium. V-MCM-41 has received many applications in oxidation reactions [3, 30–32]. For ordered mesoporous V-MCM-41 materials synthesized by DHT method [3, 25, 31], vanadium occurs mainly as isolated tetrahedrally coordinated V^{5+} species incorporated in the pore wall or anchored to the pore wall. UV–Vis spectra reveal that all the samples prepared with low V contents present well-dispersed V species in the silica network as V^{5+} species. At high surface vanadium coverage, the species are substantially polymerized. The oxidation of V^{4+} species in the precursor has also been observed. The change in the UV–Vis spectra after calcination was due to the modification in the oxidation state of vanadium (V^{5+}) from the isolated tetrahedral coordination to its distorted octahedral coordination by coming into contact with the water molecules in the atmosphere [31]. Shylesh et al. [32] reported that UV–Vis spectra of VMCM-41-DHT materials showed vanadium incorporated into the framework positions for VMCM-41 samples, while the greater percentage of active species resides on the surface of VMCM-41, enhancing the formation of higher coordinated vanadium species after calcination. Treating MCM-41 with an aqueous or alcoholic solution of vanadyl acetylacetonate can lead either to a grafting of vanadium entities on the silica surface or to an ion exchange between surfactant molecules and vanadium cations in solution. The UV–Vis spectra of the samples prepared in water or alcohol with low V contents (V/Si < 0.1) showed essentially two absorption bands at 275 and 345 nm. The first was assigned to V^{5+} species inside the silica walls, whereas those corresponding to the band at 345 nm located on the surface of the mesopores. The presence of internal sites is due to the reorganization of the hexagonal tubular structure of MCM-41 upon hydrothermal treatment, during which vanadium species are allowed to penetrate the silica walls. Thus, vanadium species in the samples obtained by impregnation are dispersed on the wall surface while in the samples obtained by direct synthesis they were fixed in

the mesoporous framework. Therefore, the surface vanadium species supported on silica are well known to possess an isolated and distorted VO_4 structure with a single V═O terminal bond and three V–O–Si bridging bonds anchored on silica support. The distorted V^{5+} species with the bridging V–O–Si could be found in different silica environments. The formation of vanadium oxide nanodomains has also been evidenced by ESR spectroscopy. A quantitative measurement of the ESR signal intensity shows that the corresponding V^{4+} species represent only 0.1% of the total V species. The majority of the species are V^{5+}. The others species are VO^{2+} which are very well dispersed and isolated inside the pore channels of MCM materials. Raman and UV–Vis spectroscopic characterization of V-MCM-41 materials were used [33] to obtain more definitive information about the possible presence of XRD-amorphous crystalline V_2O_5 nanoparticles and surface VO*x* species for samples possessing with higher vanadium content (up to 5.3 wt. %V). DR UV–Vis spectra of Me-MCM-41 (Me = Ti, V, Cr) samples obtained by direct synthesis [34] sustained the framework incorporation of Ti^{4+} ions in the inorganic silica matrix with tetrahedral or octahedral coordination, vanadium (V^{5+}) isolated species with tetrahedral environments and monochromates, with minor amounts of dichromates as well as polychromate species, respectively. The calcination treatments had changed all the Cr(III) ions to Cr(VI). A large part of these species resided on the surface of silica mesoporous support. These results indicated that the major species formed on the Cr-MCM-41 sample were monochromates, with minor amounts of dichromates as well as polychromate species. The ESR spectrum of as-synthesized chromium-containing mesoporous silica indicated, for a large part of chromium, the presence of trivalent chromium (Cr^{3+}) in octahedral coordination.

The surface vanadium species supported on silica were well known to possess an isolated and distorted VO_4 structure with a single V═O terminal bond and three V–O–Si bridging bonds anchored on silica support. The distorted V^{5+} species with the bridging V–O–Si can be found in different silica environments. Similar studies on the surface Nb^{5+} species present in Nb–MCM-41 have revealed that the Nb atoms were predominately isolated NbO_4 species under dehydration conditions, and surface polymeric niobium species and/or bulk Nb_2O_5 are formed at high niobium loading on silica [35]. Raman spectra of Ta-MCM-41 mesoporous materials indicated [6] that the incorporation of Ta atom into the MCM-41 structure forms a distorted and isolated [TaO_4] surrounded by the [SiO_4] tetrahedrons with the presence of Ta–O–Si bridging bonds, and three types of tantalum oxide species: an isolated TaO_4 species in the MCM-41 framework, an isolated surface TaO_4 species on the MCM-41 surface, and bulk Ta_2O_5, can be present individually or coexist on the Ta–MCM-41 catalysts, and it's relative intensity was dependent on the Ta concentration.

The idea of the MCM-41 impregnation with vanadium and antimony sources was to locate Sb-V-Ox species on the high surface area of mesoporous materials with various compositions [36]. Vanadium species in the prepared samples have been estimated by UV–Vis and ESR spectroscopic study. All mesoporous matrices modified with vanadium and antimony gave rise to well-resolve signals in the hyperfine structure of ESR spectra characteristic for isolated VO^{2+} species. Such a structure was not registered in the case of V/SiO_2 sample suggesting that mesoporous support was important for the isolation of oxovanadium species. Tetrahedrally coordinated vanadium (IV) species were deduced from UV–Vis spectra on all prepared samples. They were the only registered species on SbV/NbMCM-41 and SbV/AlMCM-41, whereas on SbV/MCM-41 and SbV/SiO_2, octahedral ones were also present besides them. Octahedral coordination dominated in bulk SbVOx.

There are many studies on cobalt incorporation in mesoporous silica supports. The information about the nature, the co-ordination, and the location of the metal

species for cobalt- and cobalt-vanadium-modified MCM-41 materials obtained by direct synthesis were obtained by TPR, DR-UV–Vis, and XPS analysis [25]. These methods indicated different localization of the cations in extra-framework positions or in the framework of MCM-41molecular sieves. DR-UV–Vis spectra from **Figure 3A** show two different types of V^{5+} species. The first one was assigned to isolated tetrahedrally coordinated V^{5+} species and the second originates from polymeric tetrahedral V^{5+} species grafted on the walls. According to these results, H_2-TPR measurements (**Figure 3B**) suggested that the vanadium interaction with MCM-41 was predominant in VCoMCM-41 samples and pointed to the presence of monomeric or low oligomeric dispersed tetrahedral vanadium species obtained by direct synthesis and the formation of less reducible "polymeric-like" vanadium species by postsynthesis. In the low-loaded cobalt catalysts, Co^{2+} in tetrahedral position was observed. The increase in metal content led to the appearance of Co^{3+} in Oh symmetry. In both cases, the cobalt ions were placed outside of the silica framework. In the bimetallic samples, vanadium was incorporated inside the framework of the molecular sieves and on the channel walls. V^{5+} was in tetrahedral symmetry. In the bimetallic samples, cobalt was presented as Co^{2+} in Td symmetry. When Co and V were introduced together in the starting gel, a lower quantity of vanadium was incorporated into the mesoporous sieve. At a low vanadium concentration, the essential part of cobalt gives rise to the cobalt silicate phase. The latter was reduced at higher temperature. The rest of cobalt forms CoO particles interacting weakly with the siliceous framework reduced at lower temperature. The peak at 710 K for VCo3 sample was most likely the composite one from the reduction of both cobalt and vanadium species.

Impregnation of MCM-41 and SBA-15 materials using aqueous solutions of cobalt nitrate has a significantly different impact on their ordered mesoporous structures. Thus, aqueous impregnation of MCM-41 followed in the surface area and pore volume. By comparison, SBA-15 mesoporous structure remained almost intact after the introduction of significant amounts of cobalt (up to 20%). The different behavior of these two mesoporous silicas was principally attributed to the different pore wall thickness in MCM-41 and SBA-15. Cobalt oxide-modified SBA-15,

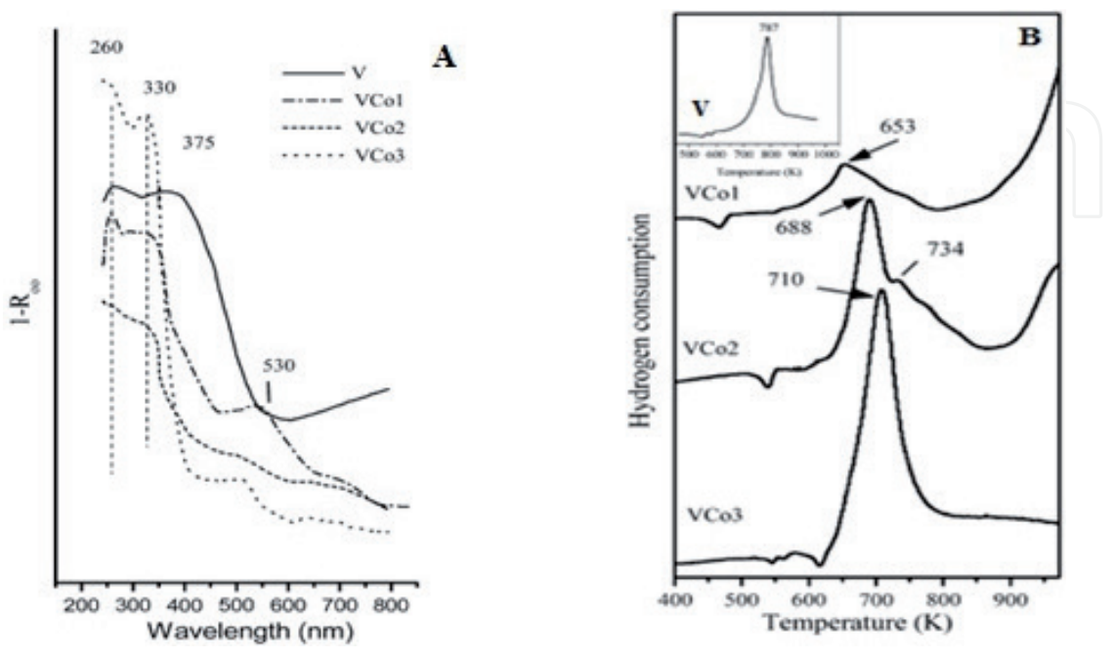

Figure 3.
DR-UV–Vis spectra (A) TPR profiles (B) of VCo-MCM-41 and V-MCM-41 samples (with permission from Ref. [25]).

KIT-5, and KIT-6 mesoporous silicas with different pore size/pore entrances have been synthesized by a conventional wet impregnation method using cobalt nitrate as the precursor. UV–Vis spectra indicated the formation of Co_3O_4 particles with different degree of dispersion, which are in different interaction with the support [2]. XPS spectra showed the variation of surface Co dispersion with aging temperature that facilitated cobalt species migration and agglomeration through the larger pores of the silica matrix. The effect of the pore size was less pronounced for the SBA-15 materials, where the straight cylindrical pores with 2-D arrangement probably leads to homogeneous distribution of the loaded cobalt oxide particles along the pore surface. For the 3D structures with interpenetrated cylindrical mesopores (KIT-6) or cage-like mesopores (KIT-5), the formation of homogeneously dispersed spinel Co_3O_4 species seems to be facilitated in mesoporous silicas with pores larger than 6 nm. TPR-DTG results evidenced the co-existence of three types of Co_3O_4 particles for all cobalt-modified SBA-15, KIT-5, and KIT-6 materials. The first type was easily reducible, relatively larger species, loosely interacting with the support; the second type represented hardly reducible and well-dispersed fraction in a moderate interaction with the silica, and the third type was very finely dispersed, strongly interacted with the support, which could not be reduced up to 873 K. The pronounced differences were observed for Co/KIT-6 materials [2]. Therefore, Co/KIT-6 samples presented a significant portion of crystalline species that weakly interacted with the support. For the KIT-6 aging to higher temperature, the presence of more inhomogeneously dispersed cobalt oxide particles, which were not completely reduced to metallic cobalt in the temperature interval 500–750 K, was revealed. For these materials, TPR-DTG analysis in correlation with the FTIR measurements supported formation of spinel-type Co_3O_4 species in the case of silicas with larger mesopores. The incorporation of Co and/or Fe in HSM and SBA-15 was evidenced by association of XRD, TEM, and TPR techniques [37]. Low-angle XRD patterns indicated that the mesoporous supports remained unchanged after metal impregnation and calcination steps; hence, still retained the ordered structure.

Iron is an interesting metal regarding its properties and applications in catalytic oxidation. In case of its immobilization in mesoporous silica by direct synthesis and hydrothermal treatment [4, 32, 38, 39], most of iron species exist in the tetrahedral coordination located in the support framework. The results obtained from DRUV–Vis, ESR, and XANES showed iron in a mixed environment, indicating that some iron was tetrahedrally coordinated, being sited in the framework, and some iron is present as an extra-framework atom, being octahedrally coordinated [38]. XANES results also suggested that copper was present in the Cu–Al-MCM-41 samples both in the framework and in the extra-framework sites as hydroxide and oxide, respectively. ESR spectra of hierarchical silica structures confirmed the presence of Fe^{3+} ions with tetrahedral coordination both in framework and extra-framework support. For samples with higher loading, the presence of interstitial oxide phase and iron oxide clusters was displayed [28]. Similar results were obtained for copper. XANES results also suggested that copper is present in the Cu–Al-MCM-41 samples both in framework and extra-framework sites as hydroxide and oxide, respectively. The presence of Al^{3+}-sites on the surface of the support provides considerably better dispersion of copper [26, 40]. When comparing ZnAl-MCM-41 with FeAl-MCM-41 samples, the interaction between the metal and the framework atoms (Zn...Si) was different. 27Al-MASNMR results have indicated that zinc is not substituted for aluminum, which means taking the EXAFS results into account that zinc (II) substitutes for silicon (IV) in the framework. The presence of several, and probably different, silicon-sites in the mesoporous framework explains the higher disorder in Zn–Al-MCM-41 compared to Fe–Al-MCM-41, in which iron substitutes for aluminum.

The incorporation of Ce, another trivalent metal, within the MCM-41 was favored by the greater flexibility of the silica network. However, the size incompatibility between Ce^{3+} and Si^{4+} ions led to longer Si\O\bonds and caused the strain bond angle in the substituted silica network. Also, the incorporation of Ce induced a drastic reduction in mesopore ordination. These results were probably due to partial substitution of the structural Si^{4+} for the Ce^{3+} ion, resulting a substantial change in the textural properties of the hexagonal structure of MCM-41 [41]. The Si/Ce molar ratio is a key factor influencing the textural properties and structural regularity of CeMCM-41 mesoporous molecular sieves. As well, XRD, UV–Vis, and XPS spectra evidenced the presence of cerium species as tetra-coordinated Ce^{4+}/Ce^{3+} and the formation of CeO_2. This was in accord with results obtained on cerium incorporated in SBA-15 [42] and KIT-6 mesoporous silica [16]. The effect of pH on SBA-15 ordered hexagonal structure and incorporation of Ce species was evidenced [42]. For the samples synthesized at pH = 10.0, the position of Ce species was evidenced as deposits only on the surface of SBA-15.

High metal dispersion and incorporation of Ni in MCM-41 framework was evidenced for lower metal loading. Typical XRD diffractograms for ordered hexagonal mesoporous structure, obtained at small angle, evidenced decreasing of structural regularity with metal loading. Considering UV–Vis of NiO as reference, a distorted tetrahedral environment was observed for the most of Ni species in these MCM-41 materials. The effect of Zr^{4+} on Ni^{2+} local symmetry and the presence of distorted tetrahedral Ti species were evidenced by UV–Vis for Ni-ZrMCM-41 and Ni-TiMCM-41 bimetallic samples. Thus, a small shoulder at around 293 nm was assigned to penta- or octahedral coordinated Ti species, resulting from the interaction of Ti species with Ni species [27]. For Ni–MnMCM-41 sample, it was assumed that both tetrahedral and octahedral Mn^{3+} species co-exist. Mn^{3+} was evidenced both in tetrahedral and octahedral coordination. The results obtained for bimetal samples were compared with them with single metal. Such for Mn-MCM-41 sample, XRD patterns showed the absence of the diffraction peaks of the MnOx species suggesting that a strong interaction between MnOx and silica matrix exists because most of the Mn^{3+} or Mn^{2+} cations were either incorporated into the silica framework or highly dispersed on the silica walls. The TPR results on Mn-MCM-41 samples [43] indicated the coexistence of different manganese species. In the samples of different pore dimensions and manganese loadings prepared by impregnation, the nature of the species, identified as well dispersed, strongly interacting with silica surface was similar. In the case of samples prepared by the hydrothermal method, the effect of pore dimensions was more complex. Narrow pores of silica materials caused the formation of small species strongly interacting with silica surface or incorporated into the framework. An increase in Mn loading and pore diameter favored formation of larger particles weakly interacting with silica support. It was observed that the presence of small oxide species of the size partially controlled by pore dimension or preparation method, and simultaneously not strongly interacting with silica support.

The incorporation of larger species into the silica framework was hindered and the formation of extra-framework oxide species was favored. Regarding the incorporation of tungsten species into the MCM-41 framework, there is a critical value for the Si/W ratio of about 30. In the case of smaller Si/W ratio, the formation of extra-framework tungsten oxide species was observed [44]. Variation of the Si/W ratio and the synthesis method has led to various species of W immobilized on HMS silica [45]. Thus, through Raman spectroscopy, isolated $[WO_4]^{2-}$ or low condensed oligomeric framework species were displayed. Tin is another metal with redox properties and large size which forms SnO_2 clusters distributed on the external pore structure. SnO_2 agglomerates were highlighted in the channels or on

the external surface, which blocked the pores partially, thereby reducing the surface area. By adjusting the nH_2O/nHCl molar ratio, Sn was incorporated into the lattice of SBA-15 at a low Sn concentration [46]. The Sn^{4+} ions exhibited both tetrahedral and octahedral coordination depending upon the location of these ions either on the walls of the silica or in the corona region of the structure, respectively. The existence of isolated oxide species that have degraded the ordered structure of the silica support and especially the formation of the oxide agglomerations in the pores or on the external surface has been highlighted for other metals with large diameter (Ru, La) but very active in oxidation reactions [24, 47–50].

The imobilization of active metals in the specific locations of ordered mesoporous silicas by direct synthesis routes with the help of organic groups of surfactants brought a new aspect of creating metal-functionalized OMSs [51]. Although the strong interactions between active metals and support were obtained, the controllable morphology and structure of OMSs synthesized by these direct synthesis routes have not been well developed. The synergistic effect between loccation, its dispersion, and mesoporous ordered silica structure on the metal electronic properties and catalytic needed development of the advanced characterization techniques.

3. Catalytic oxidation of organic compounds

The introduction of the metal cations in the mesoporous silica generated both acid and redox centers depending on their charge and their chemical properties. In oxidation reactions, these properties determine both the activity and the selectivity of the catalyst. To introduce the redox active sites in the OMSs, various transition metals have been chosen. The supports like M41S, SBA-n, and KIT-n families modified by incorporation of one, two, or more transitional metals such as Ti, V, Cr, Fe, Co, Ni, Mn, Cu, La, Ru, Ni–Ru, Cr–Ni, V–Cu, and V–Co created materials with new redox and acidic properties. The introduction of active transition metal into the framework of molecular sieves creates isolated metal sites and these centers are believed for their exceptional catalytic activity. Their catalytic properties were influenced by localization and surroundings of the metal ions. The high dispersion of metals on a support with high surface area, large pore diameter, and uniform pore size distribution determined the formation of new active centers with redox properties different from those of the oxide in the agglomerated form. This explained the increased interest in them and their applications as catalysts.

Table 1 shows a wide range of metals incorporating in mesoporous silica supports with catalytic applications in liquid phase oxidation of organic compounds, with H_2O_2 or *tert*-butyl hydroperoxide, and gas phase with O_2 from air. Various publications have shown the effects of metals and their associations with silica support and other metal on catalytic activity and selectivity. Thus, a high variety of transition-metals incorporated in mesoporous silica showed interesting catalytic properties in oxidation of organic compounds. Among them, vanadium and titanium were mostly used both single as well as associated with other metals. Vanadium-containing mesoporous materials are found to be active in liquid-phase oxidation reactions as oxidation of cyclohexane to cyclohexanone and cyclohexanol [31], oxidation of aromatic hydrocarbons and alcohols [3] using H_2O_2 as oxidant. V-MCM-41 catalysts exhibited low activity in the oxidation of alcohols but higher activity and selectivity in oxidation of cyclohexene and aromatic hydrocarbons. This suggested the association of vanadium with another metal more suitable for other oxidation reactions [21, 24]. V-TiMCM-41, V-CoMCM-41 catalysts were used in oxidation of aromatic hydrocarbons and alcohols [21, 24]. In these reactions, FeMCM-41, CoMCM-41, NiMCM-41 [3], NbMCM-41, Nb-TiMCM-41, Co-(Nb,

Catalyst	Reaction
VMCM-41	Oxidation of cyclohexane to cyclohexanone and cyclohexanol [31], oxidative dehydrogenation of propane (O_2 and N_2O as oxidant) [33]
V-MoMCM-41, Cu-FeMCM-41	Oxidation of o-xylene to phthalic anhydride in air [1], oxidation of adamantane with H_2O_2 [39]
VMCM-41, FeMCM-41, CoMCM-41, NiMCM-41	Oxidation of aromatic hydrocarbons and alcohols with H_2O_2 [3, 4, 30, 32]
VMCM-41, NbMCM-41, V-TiMCM-41, Nb-TiMCM-41, Co-(V,Nb,La)MCM-41, V-CoMCM-41	Oxidation of aromatic hydrocarbons and alcohols [21, 24]
MeMCM-41 (Me = V, Fe, Co, Ni), WHMS	Oxidation of styrene and benzene with H_2O_2 [4, 45]
Ru-(Cr, Ni, or Cu) MCM-41,La-(Co or Mn) MCM-41	Oxidation of aromatic hydrocarbons with H_2O_2 [49, 50]
MMCM-41 (M = Ti, V, Cr)	Oxidation of ethyl benzene and diphenyl methane with H_2O_2 [34]
TaMCM-41	Oxidative dehydrogenation of propane and oxidation of methanol [6]
CeMCM-41, CeKIT-6	Hydroxylation of 1-naphthol with H_2O_2 or *tert*-butyl hydroperoxide [41], oxidation of cyclohexene [52]
M (M = Al, Zr, W, B, or P) MCM-41	Oxidation of ethane [40]
Pt-SBA-15, Pt-NH2SBA-15, Pt-CoSBA-15, Pt-Co-NH2SBA-15	3-Butene-1-ol, *cis*-2-butene-1, 4-diol, cyclohexene oxidation with H_2O_2 [11, 30]
PtSBA-15/$PtSiO_2$	Oxidation of toluene with O_2 [12]
CoSBA-15, CoKIT-5, CoKIT-6	Ethyl acetate total oxidation [2]
LaKIT-6, La-BKIT-6	Oxidation of styrene with H_2O_2 [15]
TiKIT-6, Pt-TiKIT-6, Ce-TiKIT-6, Pt-Ce-TiKIT-6,	Methane in air [16]
M/KIT-6 (M = Mn, Cu, Fe, Cr, Sn)	Catalytic combustion of chlorobenzene [18]
CuImph (Imph = bis(4-imidazolyl methyl) benzylamine) on MSNs	Oxidation of toluene in air [19]
([Cu(acac)(phen) (H_2O)](ClO_4), [Cu(acac)(Me_2bipy)](ClO_4)) on HSM or NH_2HMS	Oxidation of aromatic compounds (anisole, phenol) with H_2O_2 [20]

Table 1.
Catalytic applications of modified mesoporous silica ordered networks with transitional metal.

La)MCM-41 [21, 24, 50] and Ru-(Cr, Ni, Cu)MCM-41, La-(Co, Mn)MCM-41 [49], and WHMS were also used as catalysts [45]. It was interesting to note that samples which are active in the oxidation of styrene to benzaldehyde would be less active in the oxidation of benzene to phenol and vice versa, suggesting that active centers for oxidation of styrene might probably be different to those for oxidation of benzene. Reaction data showed that the oxidation activity is higher when H_2O_2 is used as an oxidant, acetonitrile as solvent, and V-MCM-41 as catalyst. However, the selectivity toward the desired keto derivatives (ethyl benzene to acetophenone and diphenyl methane to benzophenone) follows the order, Ti-MCM-41 > V-MCM-41 > Cr-MCM-41 [34]. The vanadium content in catalysts was evidenced as a key factor in the oxidation of styrene and the conversion increases with metal loading. However, for hydroxylation of benzene, catalysts with an ordered mesostructure presented higher catalytic activity and the V content only serves as secondary role.

It can be concluded that high vanadium content favored styrene conversion and higher ordering of mesostructure led to high hydroxylation of benzene. The higher activity of vanadium-incorporated MCM-41 compared to vanadium-grafted MCM-41 may be due to the presence of active isolated tetrahedral-coordinated vanadium ions in the framework positions. The lower activity was a result of the V–O–V bond formed for vanadium-grafted MCM-41. The difference in the selectivity of as-synthesized and calcined vanadium-grafted MCM-41 showed that apart from the active redox sites, the nature of hydrophilic–hydrophobic interactions still play an important role in selective oxidation reactions. **Figure 4** depicts the variation in styrene conversion and reaction rate as a function of reaction time. The conversion and reaction rate in oxidation of styrene were modified by the introduction mode of the H_2O_2 into reaction medium in order to find the optimal reaction conditions.

The higher conversion and reaction rates were obtained in the first period of reaction when H_2O_2 was introduced after adsorption the step (samples VTi-2 and NbTi-2). These results sustained the effect of the adsorption step on oxidation reaction confirmed, over time, by photocatalytic reactions, other oxidation processes in which both Ti and V catalysts or other transition metals with redox properties were used immobilized on mesoporous silica [7–10, 28]. An induction period was needed (VTi-1, NbTi-1catalyst) in oxidation of aromatic hydrocarbons when the oxidant, reagent, catalyst, and solvent were mixed together at the beginning of the reaction and effect of the second metal was significant. The effect of the second metal on the properties of catalysts was evidenced for others materials. Firstly, the introduction of V and La reduced sharply the conversion of styrene.

The increasing of Co/V molar ratio (decreasing V amount) led to increasing of the catalytic activity. The highest conversion was obtained for Co/V molar ratio of 3.0. On the other hand, the effect of the second metal on the reactivity was different for styrene and benzene. The introduction of V or Nb into CoMCM-41 molecular sieves decreased or increased the conversion of styrene. The effect of La on CoMCM-41 was quite surprising since the activity for oxidation of styrene and benzene decreased, implying the inhibitory effect of La for oxidation of aromatics [21, 24, 50]. The main products of reaction were benzaldehyde, for oxidation of styrene, and phenol for oxidation of benzene. After the first utilization, the separated and dried catalysts were reused. The catalytic activity of these reused catalysts increased in the second cycle of reaction and decreased after the third. It was observed that the selectivity decreased gradually with reaction time and in the second cycle of reaction. Some

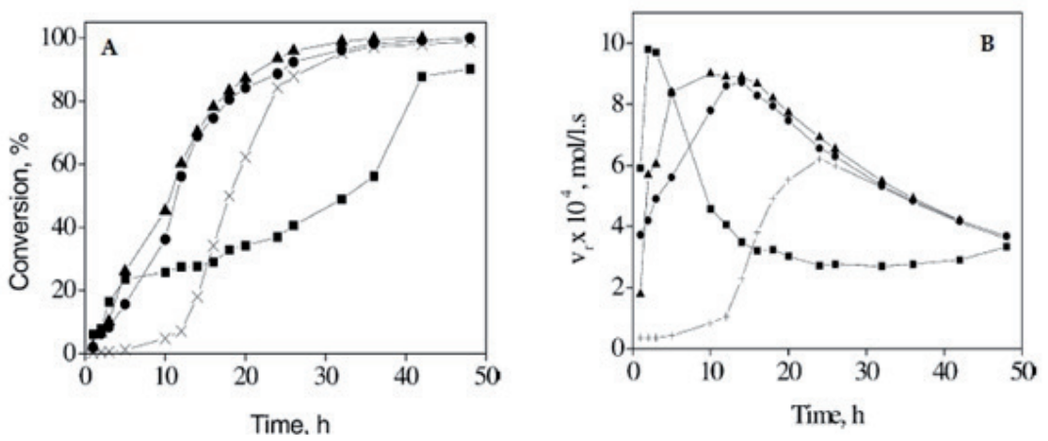

Figure 4.
Variation of the styrene conversion (A) and of the reaction rate (B) as a function of reaction time (h). VTi-1 and NbTi-1: the defined amount of H_2O_2 was introduced at the beginning of the reaction and VTi-2 and NbTi-2: the defined amount of H_2O_2 was divided in different portions and introduced step by step ((×) VTi-1, (●) VTi-2, (■) NbTi-1, (▲) NbTi-2) (with permission from Ref. [21]).

products of polycondensation resulted by polymerization of formaldehyde and/or benzaldehyde were detected after long time of reaction, a possible reason for the decrease in selectivity with reaction time. The characterization of the used and reused materials confirmed, in many cases, the good stability of bimetallic molecular sieves. TEM images of the used catalysts showed a well-ordered structure with a hexagonal arrangement of channels, indicating no effect of the reaction on the support structure after first and second reaction [24]. The IR study of adsorbed phase in discharged catalysts after first cycle reaction of styrene and benzene upon desorption at a series of temperatures (293, 373, 623, and 723 K) was made [50]. The presence of different aromatic species such as benzaldehyde and styrene glycol was observed. These species adsorbed very strongly in the catalyst since a complete desorption of these species can be made only after desorption at 723 K. The strong adsorption of these species was confirmed by thermal analysis.

The association of trivalent cations Ru or La with other transition metals modifies the activity and selectivity of the monometallic molecular sieves [24, 49]. The results evidenced that RuMCM-41 and LaMCM-41 presented good conversion in oxidation of styrene but very low activity for benzene hydroxylation. While all the bimetallic catalysts, except Ru-NiMCM-41 and La-CoMCM-41, have a higher activity and efficiency of the H_2O_2 (H_2O_2 quantity used for oxidation/H_2O_2 quantity transformed) in the benzene hydroxylation. In the styrene oxidation, only RuCr-MCM-41 gives a good conversion. Generally, excepting LaCo-MCM-41, the conversion of catalysts in oxidation of benzene was higher than that in oxidation of styrene. This behavior was specific for these bimetallic samples since all the monometallic modified MCM-41 catalysts by incorporation of the same transition metals have a higher activity in oxidation of styrene and lower conversion in hydroxylation of benzene. LaCo-MCM-41 catalyst has a very low activity and RuCr-MCM-41 catalyst has a high activity both in the styrene and benzene oxidation. Under all investigated experimental conditions for oxidation of styrene, the main reaction products detected by GC analysis were epoxy ethyl benzene (styrene oxide), phenyl ethanediol (styrene glycol), and benzaldehyde.

More transition ions were incorporated into MCM-41, HMS, SBA-15 materials, and tested in liquid-phase oxidation reactions (**Table 1**). The best activity in oxidation of benzene was obtained for Ti-MCM-41 and in oxidation of styrene for Cr-MCM-41 and CrNi-MCM-41 samples. Their activity decreases with increasing of number of 3d electrons of the metal ions. After immobilization and interaction with support and another metal, it was highlighted that increasing of their oxidation state leads to the growth of their activity. Ti, V, Cr, and Mn ions were more active. After immobilization and interaction with support and another metal, an increase of their oxidation state has been observed. The obtained redox molecular sieves by direct synthesis incorporation of tungsten into hexagonal mesoporous silica (HMS) were tested in oxidation of styrene with hydrogen peroxide. The influence of the synthesis parameters, such as, chemical composition of the gels, surfactant, precursors, and time of the hydrothermal treatment, on the structure, morphology, nature of metal species, and catalytic properties has been examined. The best results were obtained for the catalysts synthesized by oxo-polyoxo mode: $([WO(O_2)_2(H_2O)_2]/H_2O/H_3O^+/\text{surfactant}/Si(OR)_4$ in which surfactant was cetylpyridine chloride [45]. The catalysts with more ordered structure, higher surface area, and $[WO_4]^{2-}$ species strongly bounded or high dispersed on silica have a higher activity. Conversion and selectivity to benzaldehyde decreased with Si/W molar ratio (**Figure 5**). The higest conversion of styrene to benzaldehyde has been evidenced the sample with the highest amount of isolated W sites and higher surface area.

In addition to applications in the oxidation reactions [11, 24, 31], cobalt-based catalysts were considered as a suitable alternative to the high cost of catalysts based

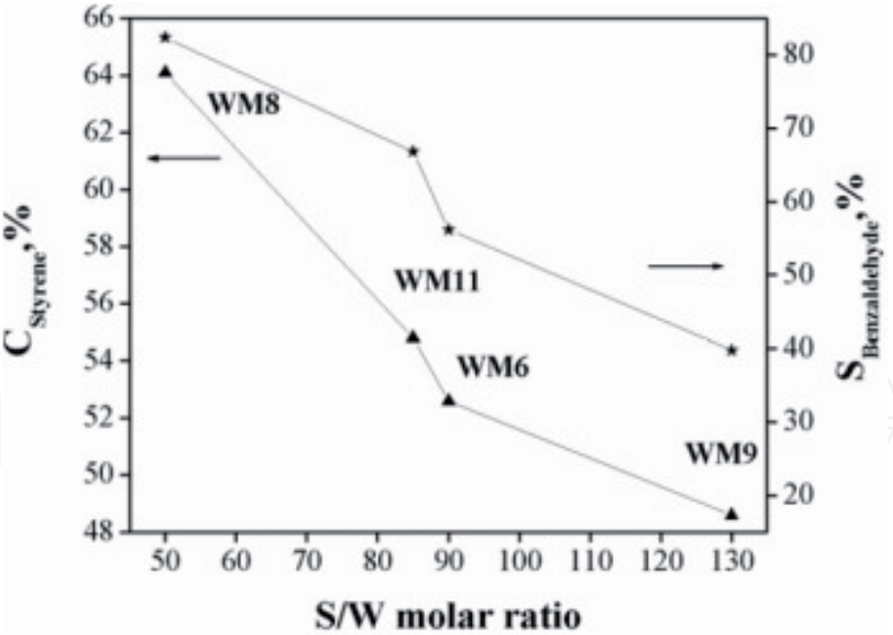

Figure 5.
Variation of conversion and selectivity with Si/W molar ratio (with permission from Ref. [45]).

on noble metals. The catalysts obtained by immobilization of Co on mesoporous silica were used for degradation of toxic compounds from the exhausted automobile and industrial emissions via combustion. Cobalt-modified SBA-15, KIT-5, and KIT-6 mesoporous silicas with different pore sizes/pore entrances have been synthesized and their catalytic activities in total oxidation of ethyl acetate were evaluated [2]. The optimal size of Co_3O_4 particles and their homogeneous distribution in the porous support are of primary importance for the catalytic activity. Silicas with larger pores facilitate the mass transfer during the sample preparation procedure and lead to more homogeneous distribution of cobalt oxide particles inside the pore system. The Co_3O_4 particle growth is facilitated by 3D structures with interpenetrating-(KIT-6) or cage-like (KIT-5) pores and much less promoted by 2D arranged straight pores of SBA-15 support.

Furthermore, more open pore structures could facilitate the catalytic process due to enhanced mass transfer, as the catalytic activity of CoKIT-6 materials is generally lower than that of CoSBA-15 and CoKIT-5.

Cerium-containing materials have been used as catalysts for selective oxidation of organic compounds. The liquid-phase oxidation of cyclohexane was carried out over Ce-KIT-6 with various Si/Ce molecular sieves at temperature between 70 and 90°C. Although the catalyst contains both Ce^{3+} and Ce^{4+}, as evidenced from DR-UV analysis, the main active sites that activate H_2O_2 were considered to be Ce^{4+} [52]. Ce^{4+} was suggested to activate hydrogen peroxide by coordination to oxidize cyclohexane, and cyclohexanol was found to be the major product (74%). Cyclohexyl acetate, as the major secondary product, was considered result of Bronsted acidity generated by Ce^{3+}. Cerium and titanium oxides, immobilized on KIT-6 silica, were used as supports for Pt. The supported Pt nanoparticles on mesoporous silica possess the ability to strongly dissociate toluene to benzene and hydrocarbon fragments (CHx) [12]. The metal–support interaction was evaluated in terms of TiO_2 loading and ceria effect on titanium oxide under condition of their dispersion on silica [16]. The highest activity was obtained in oxidation of CH_4 for all the catalyst samples containing Pt respectively for PT5K6 sample with lower dispersion of Pt and higher diameter of particles (**Figure 6**). Two opposite effects determined in this case a very small decrease in the CH_4 conversion degree

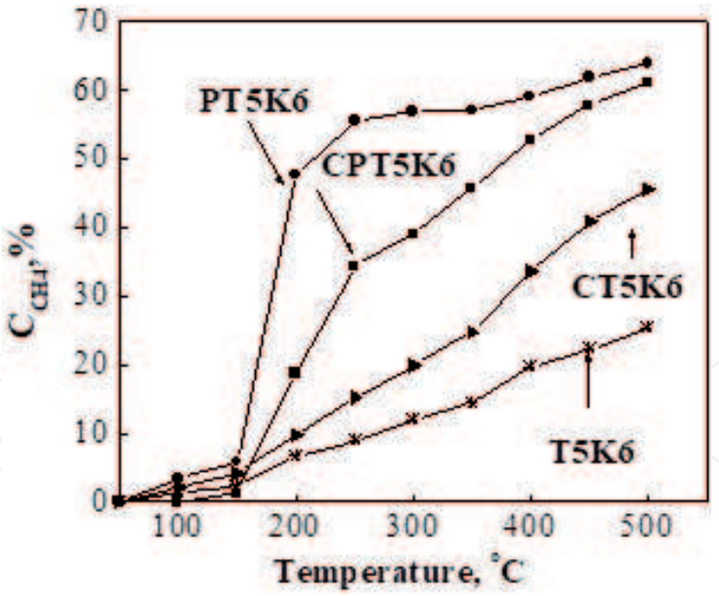

Figure 6.
CH_4 conversion and its variation with temperature for catalysts with different composition: Supported on T5K6 (a), CPTnK6 (B), and TnK6 (C) (with permission from Ref. [16]).

compared to PT5K6 catalyst. The higher concentration of Pt^{2+}on the catalyst surface (CPT4K6 samples) and absence of noble metal (CT5K6, T5K6 samples) decreased the catalytic activity and a slow growth of conversion with temperature was observed. A good correlation was obtained between catalytic activity and reducibility of the catalysts for samples with Ti and Ce. The higher conversion degree of CH_4 was obtained for PtTi-KIT-6 samples between 250 and 400°C. KIT-6 was an interesting support for other transition metals such as Mn, Cu, Fe, Cr, Sn, Ln, and the obtained catalysts were used in oxidative degradation of various organic pollutants from air (toluene, chlorobenzene) [18].

4. Incorporated metal active sites with redox properties

It can be considered that the interest on catalytic performances obtained by incorporating titanium into the zeolite (TS-1 catalyst) and the advantages of silica mesoporous molecular sieves have generated research on the metal-functionalized ordered mesoporous silicas. These catalysts have attracted much attention in the past few years for selective oxidation and oxidative photodegradation of large organic molecules. This explains the particular interest in the synthesis and use of catalysts based on titanium immobilized on various mesoporous silica substrates. The active center of TS-1 catalyst in the selective oxidation reactions was considered the titanium-isolated sites. A systematic study on the function of the different titanium species in TS-1 [53] concluded that the framework Ti species in TS-1 were the active sites for propylene epoxidation, while the nonframework Ti species were responsible for the further conversion of propylene oxide to propylene glycol and methoxy-2-propanol. Similar to TS-1, the remarkably catalytic properties of the metal-functionalized ordered mesoporous silicas result from the isolation of the metal centers in the framework. The high surface area of mesoporous sieves and the presence of ordered arrays of mesopores provide new opportunities for transition metal incorporation. It is possible to obtain metal heteroatoms as framework tetrahedral T atoms, bound in defect sites of the framework, anchored to the surface, extra-framework counter ions or extra-framework oxides.

The isolated heterogeneous single-site catalysts have been attracted great interest in diverse catalytic reactions because of their uniform and distinct geometric and electronic structure [54]. They have great potential to integrate the distinct advantages of homogeneous and heterogeneous catalysts into a single counterpart. The imobilization of active metals in the specific locations of ordered mesoporous silicas by direct synthesis routes with the help of organic groups of surfactants opened a new path in creating of metal-functionalized OMSs. Although the strong interactions between active metals and support were obtained, the controllable morphology and structure of OMSs synthesized by these direct synthesis routes have not been well developed. It is still difficult to understand the relationship between the structural morphology of OMSs and the electronic structure of active species, thus the development of advanced characterization techniques was necesary. Similar to other supported single sites [54], it can be considered that their catalytic activity is due to the following which allows: the ordered arrangement of silica support mesoporous structure; the high dispersion of metal sites, located in framework and extra-framework support, or covalently bounded on the pore surface functionalized with different ligands; the better contact of single site with the reactants thus generating catalysts with high activity and excellent selectivity; the ordered porosity can provide a special environment for the substrate interaction with the catalytic active sites which can further enhance the activity and selectivity.

Considering Ti (IV) species to be the active sites in TiMCM-41 catalyst in the oxidation of cyclohexene to cyclohexene epoxide, a mechanism in three steps was proposed for surface reaction [55]. The main reaction step involved the reaction of Ti single sites with H_2O_2 to form titanium hydroperoxide, which further reacts with cyclohexene molecules to form cyclohexene epoxide in a concerted manner. It was evidenced that titanium-isolated species from silica framework or surface were the active species. According to titanium location, two Ti-peroxide (η^1 and η^2) intermediates wherein Ti binds 1, respectively both oxygen atoms of the peroxide (**Figure 7**), have been identified.

The stability and reactivity of Ti-peroxide intermediates was affected by solvent coordination. The best results were obtained in acetonitrile. The extra-framework Ti species were amorphous or crystalline TiO_2. These species had a negative effect on the yield of propane oxide. The amorphous Ti species were more acidic and mainly responsible for the further conversion of propane oxide.

The mechanisms proposed for oxidation of organic compounds with H_2O_2 on vanadium-modified mesoporous silica supports proposed also the formation of V-peroxide intermediates (η^1 and η^2). These results were also generalized for the activity of other immobilized metals. Thus, the specific catalytic activity (per one Cu^{2+}-active site accessible to the reactants) depended strongly on the structure of

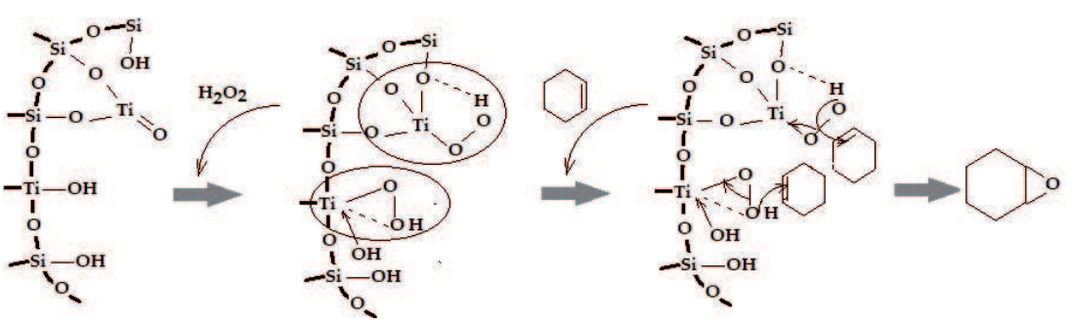

Figure 7.
The oxidation mechanism proposed for possible isolated Ti^{4+} active sites immobilized on mesoporous silica.

the localized site [40]. Isolated Cu^{2+}-sites grafted to Al-MCM-41 showed relatively high activity for the sample calcined at lower temperature. Thermal treatment at higher temperatures caused a sharp loss of specific Cu^{2+} catalytic activity of CuAl-MCM-41 as result of copper oxide agglomeration.

If the organic substrate was introduced in the first step of the reaction, it was adsorbed on the surface and reacted more rapidly with the Me-peroxide intermediate formed by the addition of H_2O_2 in the second step [21]. The presence of the organic compound on the surface prevented H_2O_2 decomposition more in the presence of extra-framework oxides that favor its decomposition. Depending of their loading and dispersion, the activity of these metal extra-framework species was similar with that of clusters or bulk oxides. For Ru- and La-incorporated MCM-41 molecular silica, the ratio of metal and oxygen ion radii ($RM(n^+)/RO(2^-) > 0.5$), an important structural parameter, showed a little possibility to be incorporated metals in the silica framework [49]. For many of these catalysts, the efficiency of the H_2O_2 (H_2O_2 quantity used for oxidation/H_2O_2 quantity transformed) was very low. These catalysts had a good conversion in oxidation of styrene but very low for benzene hydroxylation. Their association with metals with smaller diameter as Co or Mn led to a higher activity and efficiency of the H_2O_2.

The hydrophobicity of metal-functionalized ordered mesoporous silicas was improved, in many cases, by functionalization of surface with organic groups in direct (co-condensation) or postsynthetic silylation treatment. The coexistence of metal cations with other organic or inorganic species favored the distribution on the pore surface of catalytic active species, thus favoring the access of the reactants during the chemical reaction. However, in this case, the metal species formed oxide agglomerations, which led to the decreasing of the conversion. Thus, for LaKIT-6 catalyst, the coexistence of B hindered the dispersion or incorporation of La into the framework [15]. La^{3+} species in the framework of LaKIT-6 were favorable to improve the catalytic performance of LaKIT-6 for the oxidation of styrene. When H_2O_2 was used as an oxidant, LaBKIT-6 showed much lower styrene conversion than LaKIT-6 catalyst with similar product selectivity, which was ascribed to the formation on surface of La_2O_3 nanocrystals.

The controllable dispersion of metal single sites and a higher hydrophobicity were obtained by immobilization of the metal complexes on mesoporous silica supports. A number of mono- and binuclear metal complexes have been investigated as biomimetic catalysts for organic compound oxidation. New biomimetic catalysts were obtained by immobilization of $[Cu(AcAc)(Phen)(H_2O)]ClO_4$, $[Cu(AcAc)(Me_2bipy)]\ ClO_4$ complexes on HMS or NH_2-functionalized mesoporous silica [20]. The copper-substituted mesoporous silica was a good catalyst for oxidation of aromatic compounds or a very good support for biomimetic oxidation catalyst due to the possible interactions between the metallic ions of the biomimetic complex and the stabilized cuprous species in the silica framework. The immobilization on different mesoporous silica supports of (Schiff base) copper(II) or Mn(II) complexes was synthesized and applied in oxidation of alcohols in acetonitrile and H_2O_2. Comparing the effect of silica supports on catalytic activity, the higher performances of the metal complexes supported on MCM-41 were evidenced. A higher catalytic activity was obtained for Mn complexes, especially in oxidation of cyclohexene in conditions of significant lower M/L ratio and metal content. The most probable mechanism for attachment of the aminopropyl groups to the surface of mesoporous silicas was proposed through siloxane linkages (Si–O–Si) between the silicon of the aminopropylsilane group and the surface silicon atoms. It has been assumed the possibility that each aminopropylsilane silicon attaches to the internal surface of the silica via one, as well two and/or three siloxane linkages. **Figure 8** proposes the metal complex structure immobilized on SBA-15 mesoporous support.

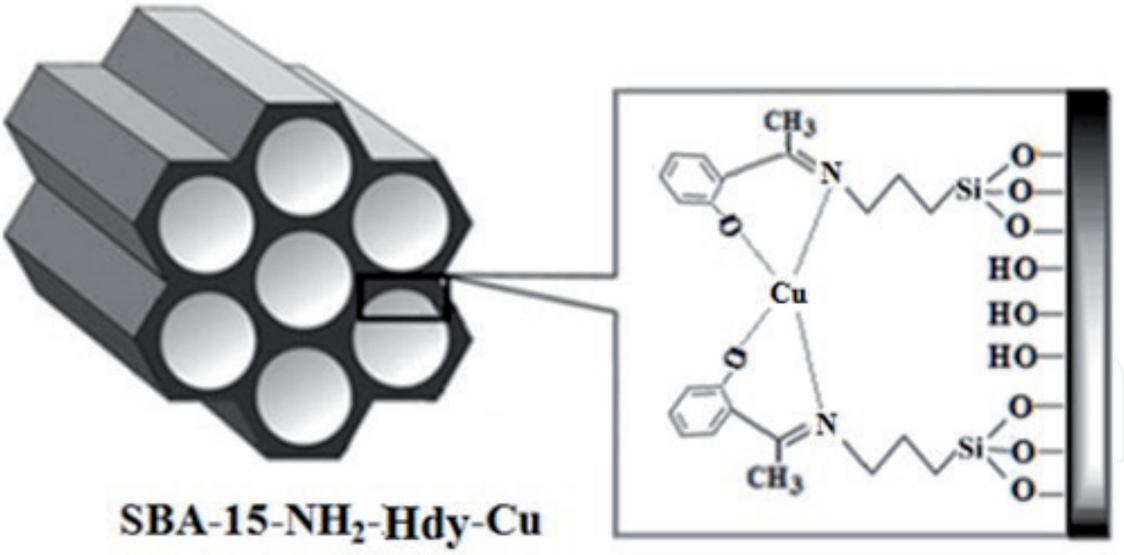

Figure 8.
Copper single site supported by complexation with Schiff-base ligands obtained from 2-hydroxyacetopheneone covalently attached to amino-functionalized SBA-15 (unpublished).

The stability and heterogeneous nature of these catalysts in the oxidation of different substrates have been investigated. The oxidation in the liquid phase with organic hydroperoxides or even H_2O_2 was often the subject of leaching phenomena and the question about the true nature of the catalytic reaction (homogeneous or heterogeneous) was a serious one.

The photocatalytic activity of supported transition metals (Ti, V, Ce, Fe, Cu, Au, Ag, Ta, Nb) on mesoporous silica supports in mono- or bimetallic photocatalysts was evaluated in degradation of various organic pollutants from water or air. Among the various mesoporous silica materials, MCM-48 and KIT-6 were several advantages in photocatalysis due to their cubic arrangement of the three-dimensional mesopores and their considerable amount of surface silanol groups. The photocatalytic properties of CeTi-MCM-48 photocatalysts were evaluated by phenol photodegradation under UV irradiation at two different wavelengths and the photocatalytic activity was correlated with the active metallic distribution, speciation, and their immobilization method [7, 8]. The incorporation of Ce in the Ti-MCM-48 framework allowed activation by UV light, generating more electrons and holes in the photocatalytic redox reactions and a better photoactivity for phenol. The presence of redox couple Ce^{4+}/Ce^{3+} exchaged the surface oxygen vacancies that could be transformed in oxygen radicals with formation of superoxide radicals. Many other photocatalysts were obtained by immobilization of the photoactive transition metals on various mesoporous silica supports, and their activity was evaluated in oxidation of organic polutants from water as dyes, functionalized 8-hydroxyquinolinate, antibiotics [9, 10, 28, 56]. In all of these, the active photoactive metallic sites were Ti^{4+}, Co^{2+}, Fe^{3+}, Al^{3+}, Zn^{2+}, Eu^{3+}, Tb^{3+}, Er^{3+}, Nd^{3+} with various dispersion on MCM-41, SBA-15 or hierarchical silica supports.

In case of the catalysts used in gas-phase reactions, dispersion, specific surface area, and reducibility was observed as the main factors influencing the catalytic activity. In combustion of chlorobenzene (CB), catalytic activity of metal-modified KIT-6 (M = Mn, Cu, Fe, Cr, Sn) mesoporous catalysts was basically in line with their redox properties, with the exception of CrKIT-6, which differs from this trend due to the aggregation of Cr species in the pore structure and surface of the KIT-6 [18]. The proposed mechanism was follows: CB was adsorbed to the catalyst by physical adsorption, then the adsorbed CB molecule dissociated

on the active sites (mainly metal oxides) via nucleophilic attacks on C–Cl bond. The results obtained showed decreasing catalytic activity in the following order: MnKIT-6 > CrKIT-6 > CuKIT-6 > FeKIT-6 > Sn/KIT-6, in correlation with redox properties of the catalysts. Therefore, the best catalytic combustion activity of MnKIT-6 catalysts benefited from their large specific surface area, good Mn dispersion, better reducibility, and large amount of chemisorbed oxygen species. However, as the content of Mn species increasing, due to increased agglomeration of Mn, more MnOx clusters gave rise to pore plugging and cover adsorption sites, leading to weaker catalytic activity. Mesoporous silica KIT-6 with 3D interconnected mesopores offered a confined environment, a better dispersion of the oxide phase, and a faster diffusion of the reactants and products. The Mo/KIT-6, Fe/KIT-6, and Mo–Fe/KIT-6 were tested as potential alternatives to noble metals in the conversion of MCP [57]. Only the isolated tetrahedral Fe ions and highly dispersed small FeOx nanoclusters were responsible for the endocyclic C-C bond rupture at substituted C-C. The synergy between Fe and Mo was not observed at low temperatures and for total conversion but only for ring-opening reactions at higher temperature.

In particular, the good performance of the Ti(IV)-doped SBA-15-supported catalysts in CH4 oxidation was due to the combination of Ti(IV) structurally incorporated into the silica lattice and present as surface-dispersed TiO_2 particles. The negative effect of the Ti(IV) over the HMS-supported catalysts was related to the high acidity induced by the more homogeneous incorporation of Ti(IV) into the silica structure. The loss of catalyst activity during CH_4 oxidation reaction was not necessarily related to the sintering of the active sites but rather to the variation of the oxygen storage capacity and oxygen mobility strictly related to the support properties. For PdTi-SBA-15 catalysts, combustion of methane occurs through a redox or Mars van Krevelen mechanism was accepted [58]. Accordingly, during this reaction, PdO was locally reduced to Pd by methane, producing H_2O and CO_2, and then Pd was reoxidized by oxygen. Although the active species was considered PdO, it was widely recognized that metallic Pd plays the important role in decomposing and activating the methane molecule. Similar conclusions were obtained also for PtTiKIT-6 catalysts [16]. Therefore, the efficiency of all process was related to the redox properties of the catalyst and to the oxygen mobility. The maintenance of the activity, in spite of the significant palladium oxide sintering, was attributed to the good interaction between surface titania and silica. Such interaction favored the formation of Ti–O–Si linkages with an increase of the oxidizing potential of the Ti(IV) cations. In the presence of a support metal interaction, the increase of the PdO particle size [58], respectively PtO [16] after the long reaction is not detrimental. Another effect of metal–support interaction was observed for Ce-TiKIT-6 samples. In this case, two factors were influencing the Pt activity: dispersion and size of the platinum species and their concentration on the surface. Two opposite effects determined a decreasing in the CH_4 conversion. The higher concentration of Pt^{2+} and lower Pt^0 concentration on the catalyst surface. A good correlation was obtained between catalytic activity, and reducibility of the catalysts was also obtained for samples with Ti and Ce supported on KIT-6.

5. Conclusions

It can be concluded that OMSs containing transition metals showed extremely promising redox properties in the oxidation of organic compounds with larger molecules thanks to the mesoporous support. The applications and performances of the redox couple diversity resulted by association of transition metals on an increasing

diversity of mesoporous or hierarchical ordered structures based on silica offer new research directions in this field. However, the decoration of multiple metal active species and their synergistic interactions on the surface of mesoporous silica remain to be explored in the future.

Author details

Viorica Parvulescu
Institute of Physical Chemistry "Ilie Murgulescu" of the Romanian Academy, Bucharest, Romania

*Address all correspondence to: vpirvulescu@icf.ro

References

[1] Selvaraj M, Lee TG. A novel route to produce phthalic anhydride by oxidation of o-xylene with air over mesoporous V-Mo-MCM-41 molecular sieves. Microporous and Mesoporous Materials. 2005;**85**:39-51. DOI: 10.1016/j.micromeso.2005.05.046

[2] Tsoncheva T, Ivanova L, Rosenholm J, MikaLinden M. Cobalt oxide species supported on SBA-15, KIT-5 and KIT-6 mesoporous silicas for ethyl acetate total oxidation. Applied Catalysis B: Environmental. 2009;**89**:365-374. DOI: 10.1016/j.apcatb.2008.12.015

[3] Parvulescu V, Anastasescu C, Su B-L. Vanadium incorporated mesoporous silicates as catalysts for oxidation of alcohols and aromatics. Journal of Molecular Catalysis A: Chemical. 2003;**198**:249-261. DOI: 10.1016/S1381-1169(02)00694-5

[4] Parvulescu V, Su B-L. Iron, cobalt or nickel substituted MCM-41 molecular sieves for oxidation of hydrocarbons. Catalysis Today. 2001;**69**:315-322. DOI: 10.1016/S0920-5861(01)00384-4

[5] Yang Y, Lim S, Wang C, Harding D, Haller G. Multivariate correlation and prediction of the synthesis of vanadium substituted mesoporous molecular sieves. Microporous and Mesoporous Materials. 2004;**67**:245-257. DOI: 10.1016/j.micromeso.2003.11.010

[6] Jehng J-M, Tung WC, Huang C-H, Wachs IE. Structural characteristics and reactivity properties of the tantalum modified mesoporous silicalite (MCM-41) catalysts. Microporous and Mesoporous Materials. 2007;**99**:299-307. DOI: 10.1016/j.micromeso.2006.09.036

[7] Mureseanu M, Parvulescu V, Radu T, Filip M, Carja G. Mesoporous CeTiSiMCM-48 as novel photocatalyst for degradation of organic compounds. Journal of Alloys and Compounds. 2015;**648**:864-873. DOI: 10.1016/j.jallcom.2015.07.078

[8] Mureseanu M, Filip M, Somacescu S, Baran A, Carja G, Parvulescu V. Ce, Ti modified MCM-48 mesoporous photocatalysts: Effect of the synthesis route on support and metal ion properties. Applied Surface Science. 2018;**444**:235-242. DOI: 10.1016/j.apsusc.2018.03.053

[9] Kong L-L, Yan B, Li Y-J, Li Y. Photoactive metallic (Al^{3+}, Zn^{2+}, Eu^{3+}, Tb^{3+}, Er^{3+}, Nd^{3+}) mesoporous hybrid materials by functionalized 8-hydroxyquinolinate linkage covalently bonded SBA-15. Microporous and Mesoporous Materials. 2010;**135**:45-50. DOI: 10.1016/j.micromeso.2010.06.009

[10] Suraja VP, Yaakob Z, Binitha NN, Resmi MR, Silija PP. Photocatalytic degradation of dye pollutant over Ti and Co doped SBA-15: Comparison of activities under visible light. Chemical Engineering Journal. 2011;**176-177**:265-271. DOI: 10.1016/j.cej.2011.05.071

[11] Niculescu V, Aldea N, Rednic V, Parvulescu V. Platinum mesoporous silica catalysts for liquid media oxidation. Analytical Letters. 2019;**52**:5-19. DOI: 10.1080/00032719.2017.1421214

[12] Lai YT, Chen TC, Lan YK, Chen BS, You JH, Yang CM, et al. Pt/SBA-15 as a highly efficient catalyst for catalytic toluene oxidation. ACS Catalysis. 2014;**4**:3824-3836. DOI: 10.1021/cs500733j

[13] Kim TW, Ryoo R, Kruk M, Gierszal KP, Jaroniec M, Kamiya S, et al. Tailoring the pore structure of SBA-16 silica molecular sieve through the use of copolymer blends and control of synthesis temperature and time.

The Journal of Physical Chemistry. 2004;**108**:11480-11489. DOI: 10.1021/jp048582k

[14] Karthikeyan G, Pandurangan A. Post synthesis alumination of KIT-6 materials with Ia3d symmetry and their catalytic efficiency towards multicomponent synthesis of 1H-pyrazolo[1,2-]phthalazine-5,10-dione carbonitriles and carboxylates. Journal of Molecular Catalysis A: Chemical. 2012;**361-362**:58-67. DOI: 10.1016/j.molcata.2012.05.003

[15] Zhan W, Guo Y, Wang Y, Guo Y, Lu G. Synthesis of lathanum or La-B doped KIT-6 mesoporous materials and their application in the catalytic oxidation of styrene. Journal of Rare Earths. 2010;**28**:369-375. DOI: 10.1016/S1002-0721(09)60105-8

[16] Filip M, Todorova S, Shopska M, Ciobanu M, Papa F, Somacescu S, et al. Effects of Ti loading on activity and redox behavior of metals in PtCeTi/KIT-6 catalysts for CH_4 and CO oxidation. Catalysis Today. 2018;**306**:138-144. DOI: 10.1016/j.cattod.2017.02.013

[17] Ghohe NM, Tayebee R, Amini MM. Synthesis and characterization of mesoporous NbZr/KIT-6 as a productive catalyst for the synthesis of benzylpyrazolyl coumarins. Materials Chemistry and Physics. 2019;**223**:268-276. DOI: 10.1016/j.matchemphys.2018.10.067

[18] He F, Luo J, Liu S. Novel metal loaded KIT-6 catalysts and their applications in the catalytic combustion of chlorobenzene. Chemical Engineering Journal. 2016;**294**:362-370. DOI: 10.1016/j.cej.2016.02.068

[19] Liu C-C, Lin T-S, Chan SI, Mou C-Y. A room temperature catalyst for toluene aliphatic C–H bond oxidation: Tripodal tridentate copper complex immobilized in mesoporous silica. Journal of Catalysis. 2015;**322**:139-151. DOI: 10.1016/j.jcat.2014.12.005

[20] Mureşeanu M, Pârvulescu V, Ene R, Cioateră N, Pasatoiu TD, Andruh M. Cu(II) complexes imobilized on functionalized mesoporous silica as catalysts for biomimetic oxidations. Journal of Materials Science. 2009;**44**:6795-6804. DOI: 10.1007/s10853-009-3682-6

[21] Parvulescu V, Anastasescu C, Constantin C, Su B-L. Mono (V, Nb) or bimetallic (V–Ti, Nb–Ti) ions modified MCM-41 catalysts: Synthesis, characterization and catalysis in oxidation of hydrocarbons (aromatics and alcohols). Catalysis Today. 2003;**78**:477-485. DOI: 10.1016/S0920-5861(02)00330-9

[22] Amama PB, Lim S, Ciuparu D, Pfefferle L, Haller GL. Hydrothermal synthesis of MCM-41 using different ratios of colloidal and soluble silica. Microporous and Mesoporous Materials. 2005;**81**:191-200. DOI: 10.1016/j.micromeso.2005.02.001

[23] Choi KM, Tatsumi T, Yokoi T, Kuroda K. Usefulness of alkoxyltitanosiloxane for the preparation of mesoporous silica containing a large amount of isolated titanium. Journal of Colloid and Interface Science. 2011;**359**:240-247. DOI: 10.1016/j.jcis.2011.03.016

[24] Parvulescu V, Tablet C, Anastasescu C, Su B-L. Activity and stability of bimetallic Co (V, Nb, La)-modified MCM-41 catalysts. Catalysis Today. 2004;**93-95**:307-313. DOI: 10.1016/j.cattod.2004.06.006

[25] Todorova S, Pârvulescu V, Kadinov G, Tenchev K, Somacescu S, Su B-L. Metal states in cobalt- and cobalt-vanadium-modified MCM-41 mesoporous silica catalysts and their

activity in selective hydrocarbons oxidation. Microporous and Mesoporous Materials. 2008;**113**:22-30. DOI: 10.1016/j.micromeso.2007.10.047

[26] Szegedi Á, Kónya Z, Méhnb D, Solymár E, Pál-Borbély G, Horváth ZE, et al. Spherical mesoporous MCM-41 materials containing transition metals: Synthesis and characterization. Applied Catalalysis A: General. 2004;**272**:257-266. DOI: 10.1016/j.apcata.2004.05.057

[27] Yang YH, Lim S, Du GA, Chen Y, Ciuparu D, Haller GL. Synthesis and characterization of highly ordered Ni-MCM-41 mesoporous molecular sieves. The Journal of Physical Chemistry B. 2005;**109**:13237-13246. DOI: 10.1021/jp044227i

[28] Petcu G, Anghel EM, Somacescu S, Preda S, Culita DC, Mocanu S, et al. Hierarchical zeolite Y containing Ti and Fe oxides as photocatalysts for degradation of amoxicillin. Journal of Nanoscience and Nanotechnology. 2020;**20**:1158-1169. DOI: 10.1166/jnn.2019.16981

[29] Kolev H, Todorova S, Naydenov A, Ene R, Ivanov G, Parvulescu V, et al. Catalytic activity of mesoporous SBA-15 modified with Pt and Ti in a deep methane, n-hexane and CO oxidation. Athens Journal of Sciences. 2014;**1**:9-20. DOI: 10.30958/ajs.1-1-1

[30] Cánepa AL, Elías VR, Vaschetti VM, Sabre EV, Eimer GA, Casuscelli SG. Selective oxidation of benzyl alcohol through eco-friendly processes using mesoporous V-MCM-41, Fe-MCM-41 and Co-MCM-41 materials. Applied Catalysis A: General. 2017;**545**:72-78. DOI: 10.1016/j.apcata.2017.07.039

[31] Baoshan KW, Han LC, Liu J. Synthesis, characterization of MCM-41 with high vanadium content in the framework and its catalytic performance on selective oxidation of cyclohexane. Applied Catalysis A: General. 2014;**479**:70-75. DOI: 10.1016/j.apcata.2014.04.004

[32] Shylesh S, Singh AP, Shylesh S, Singh AP. Synthesis, characterization, and catalytic activity of vanadium-incorporated, -grafted, and -immobilized mesoporous MCM-41 in the oxidation of aromatics. Journal of Catalysis. 2004;**228**:333-346. DOI: 10.1016/j.jcat.2004.08.037

[33] Kondratenko EV, Cherian M, Baerns M, Su D, Schlögl R, Wang X, et al. Oxidative dehydrogenation of propane over V/MCM-41 catalysts: Comparison of O_2 and N_2O as oxidants. Journal of Catalysis. 2005;**234**:131-142. DOI: 10.1016/j.jcat.2005.05.025

[34] Jha RK, Shylesh S, Bhoware SS, Singh AP. Oxidation of ethyl benzene and diphenyl methane over ordered mesoporous M-MCM-41 (M = Ti, V, Cr): Synthesis, characterization and structure–activity correlations. Microporous and Mesoporous Materials. 2003;**95**:154-163. DOI: 10.1016/j.micromeso.2006.04.018

[35] Ziolek M, Nowak I. Characterization techniques employed in the study of niobium and tantalum-containing materials. Catalysis Today. 2003;**78**:543-553. DOI: 10.1016/S0920-5861(02)00353-X

[36] Golinska H, Decyk P, Ziolek M, Kujawa J, Filipek E. Sb-V-Ox catalysts—Role of chemical composition of MCM-41 supports in physicochemical properties. Catalysis Today. 2009;**142**:175-180. DOI: 10.1016/j.cattod.2008.10.044

[37] Braganca LFFPG, Ojedac M, Fierroc JLG, Pais da Silva MI. Bimetallic Co–Fe nanocrystals deposited on SBA-15 and HMS mesoporous silicas as catalysts for Fischer–Tropsch synthesis. Applied Catalysis A: General. 2012;**423-424**:146-153. DOI: 10.1016/j.apcata.2012.02.031

[38] Nilsen MH, Antonakou E, Bouzga A, Lappas A, Mathisen K, Stocker M. Investigation of the effect of metal sites in Me–Al-MCM-41 (Me = Fe, Cu or Zn) on the catalytic behavior during the pyrolysis of wooden based biomass. Microporous and Mesoporous Materials. 2007;**105**:189-203. DOI: 10.1016/j.micromeso.2007.05.059

[39] Parida KM, Dash SK. Adsorption of Cu^{2+} on spherical Fe-MCM-41 and its application for oxidation of adamantane. Journal of Hazardous Materials. 2010;**179**:642-649. DOI: 10.1016/j.jhazmat.2010.03.051

[40] Kucherov AV, Shigapov AN, I vanov AV, Kucherova TN, Kustov LM. Distribution and properties of catalytically active Cu^{2+}-sites on a mesoporous MCM-41 silicate modified by Al, Zr, W, B, or P ions. Catalysis Today. 2005;**110**:330-338. DOI: 10.1016/j.cattod.2005.09.031

[41] Laha SC, Mukherjee P, Sainkar SR, Kumar R. Cerium containing MCM-41-type mesoporous materials and their acidic and redox catalytic properties. Journal of Catalysis. 2002;**207**:213-223. DOI: 10.1006/jcat.2002.3516

[42] Dai Q, Wang X, Chen G, Zheng Y, Lu G. Direct synthesis of cerium (III)-incorporated SBA-15 mesoporous molecular sieves by two-step synthesis method. Microporous and Mesoporous Materials. 2007;**100**:268-275. DOI: 10.1016/j.micromeso.2006.11.015

[43] Derylo-Marczewska A, Gacb W, Popivnyak N, Zukocinski G, Pasieczna S. The influence of preparation method on the structure and redox properties of mesoporous Mn-MCM-41 materials. Catalysis Today. 2006;**114**:293-306. DOI: 10.1016/j.cattod.2006.02.066

[44] Wu H-Y, Zhang X-L, Yang C-Y, X. Chen X, Zheng X-C. Alkali-hydrothermal synthesis and characterization of W-MCM-41 mesoporous materials with various Si/W molar ratios. Applied Surface Science. 2013;270:590-595. Doi: 10.1016/j.apsusc.2013.01.090

[45] Parvulescu V, Ciobanu M, Petcu G, Anghel EM, Tungsten–modified SB-L. HMS catalysts for high selective oxidation of styrene with aqueous hydrogen peroxide. Revue Roumaine de Chimie. 2018;**63**:847-853

[46] Shah P, Ramaswamy AV, Lazar K, Ramaswamy V. Synthesis and characterization of tin oxide-modified mesoporous SBA-15 molecular sieves and catalytic activity in trans-esterification reaction. Applied Catalysis A: General. 2004;**273**:239-302. DOI: 10.1016/j.apcata.2004.06.039

[47] Kawi S, Liu SY, Shen S-C. Catalytic decomposition and reduction of N_2O on Ru/MCM-41 catalyst. Cataysis Today. 2001;**68**:237-244. DOI: 10.1016/S0920-5861(01)00283-8

[48] Jang M, Park JK, Shin EW. Lanthanum functionalized highly ordered mesoporous media: Implications of arsenate removal. Microporous and Mesoporous Materials. 2004;**75**:159. DOI: 10.1016/j.micromeso.2004.05.018

[49] Parvulescu V, Anastasescu C, Su BL. Bimetallic Ru-(Cr, Ni, or Cu) and La-(Co or Mn) incorporated MCM-41 molecular sieves as catalysts for oxidation of aromatic hydrocarbons. Journal of Molecular Catalysis A: Chemical. 2004;**211**:143-148. DOI: 10.1016/j.molcata.2003.10.011

[50] Parvulescu V, Constantin C, Su B-L. Liquid phase oxidation of aromatic hydrocarbons using highly ordered Nb and NbCo-MCM-41 nanoreactors. Journal of Molecular Catalysis A: Chemical. 2003;**202**:171-178. DOI: 10.1016/S1381-1169(03)00202-4

[51] Zhou S, Yang F, Wang B, Su H, Lu K, Din Y, et al. Oriented decoration in metal-functionalized ordered mesoporous silicas and their catalytic applications in the oxidation of aromatic compounds. Catalysts. 2018;**8**:80-110. DOI: 10.3390/catal8020080

[52] Prabhu A, Kumaresan L, Palanichamy M, Murugesan V. Cerium-incorporated cage-type mesoporous KIT-6 materials: Synthesis, characterization and catalytic applications. Applied Catalysis A: General. 2010;**374**:11-17. DOI: 10.1016/j.apcata.2009.11.016

[53] Xiong G, Cao Y, Guo Z, Jia Q, Tian F, Liu L. The roles of different titanium species in TS-1 zeolite in propylene epoxidation studied by in situ UV Raman spectroscopy. Physical Chemistry Chemical Physics. 2016;**18**:190-196. DOI: 10.1039/c5cp05268h

[54] Zhao W, Li G, Tang Z. Metal-organic frameworks as emerging platform for supporting isolated single-site catalysts. Nano Today. 2019;**27**:178-197. DOI: 10.1016/j.nantod.2019.05.007

[55] Roy SK, Dutta D, Talukdar AK. Highly effective methylated Ti MCM-41 catalyst for cyclohexene oxidation. Materials Research Bulletin. 2018;**103**:38-46. DOI: 10.1016/j.materresbull.2018.03.017

[56] Orbeci C, Stănescu R, Negoescu D, Parvulescu V. Synthesis, characterization and functionalization of MCM-41 for the removal of organic compounds from waste waters. Environmental Engineering and Management Journal. 2017;**16**:*553-560*

[57] Boulaoued A, Fechete I, Donnio B, Bernard M, Turek F, Garin F. Mo/KIT-6, Fe/KIT-6 and Mo–Fe/KIT-6 as new types of heterogeneous catalysts for the conversion of MCP. Microporous and Mesoporous Materials. 2012;**155**:131-142. DOI: 10.1016/j.micromeso.2012.01.028

[58] Venezia AM, Carlo GG, Liotta LF, Pantaleo G, Kantcheva M. Effect of Ti(IV) loading on CH_4 oxidation activity and SO_2 tolerance of Pd catalysts supported on silica SBA-15 and HMS. Applied Catalysis B: Environmental. 2011; 106:529-539. Doi: 10.1016/j.apcatb.2011.06.013